ORIGINAL ARTICLE

lajss.org© Latin American Journal of Solids and Structures

www.lajss.org

Calculation analysis on flexural performance of partially encased concrete cellular beams

Qiuyu Liu[a], Jiongfeng Liang[b]*, Bin Zou[a], Caisen Wang[c], Shengzhi Shi[d], Kai Wang[e]

[a] Nanchang Architecture Science Institute Co., Ltd., Nanchang 330096, China. Email: 1297895421@qq.com, 99781234@qq.com
[b] School of Civil & Architecture Engineering, East China University of Technology, Nanchang, 330013, China. Email: jiongfeng108@126.com
[c] College of Architecture and Civil Engineering, Beijing University of Technology, Beijing, 100124, China. Email: wcs9797@126.com
[d] China Northwest Building Design and Research Institute Co. Ltd., Xi'an 710018, China. Email: shishengzhi@126.com
[e] China Railway Construction Engineering Group Co. Ltd., China. Email: 1225000670@qq.com

* Corresponding author

https://doi.org/10.1590/1679-7825/e9060

Abstract

This study examines the flexural performance of partially encased concrete cellular beams (PECCBs), in which continuous openings are introduced into the web of the main steel component (MSC). To evaluate the influence of web openings and their geometries on structural behavior, six PECCBs with different configurations and one conventional partially encased concrete beam (PECB) were tested. The parameters investigated included three cellular geometries (circular, square, and hexagonal), two opening ratios, and three flange thicknesses. Experimental results indicated that conventional PECB specimens primarily failed through concrete crushing and flange buckling, whereas PECCBs exhibited lower flange tensile failure with concrete damage or upper flange buckling in compression. The presence of cellular webs enhanced the overall energy absorption capacity, with circular openings delivering the best performance, followed by hexagonal and square shapes. The cracking load was governed by both the opening ratio and geometry, with the highest value of 27.14 kN·m obtained for circular-cellular beams. Based on the test results, a cracking load prediction formula and an analytical deflection model were developed using the discounted web thickness method. Comparisons with JGJ 138-2016 and T/CECS 719-2020 demonstrated that the proposed deflection model achieved superior accuracy, with an average error of 4.20% and a standard deviation of 0.045.

Keywords

Calculation analysis, Flexural performance, Partially encased concrete, Main steel component, Cellular beam

Graphical Abstract

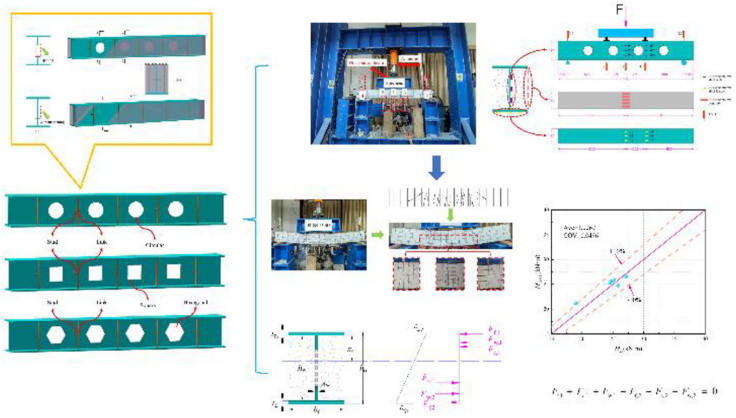

Received April 04, 2026. In revised form May 24, 2026. Accepted May 28, 2026. Available online June 08, 2026.
https://doi.org/10.1590/1679-7825/e9060

1 INTRODUCTION

Partially encased concrete(PEC) structures are a type of concrete cast in wide flange steel members (H-beams) with the web in the concrete and the wide flange on the outside(Ebadi Jamkhaneh et al.2019, Mucedero et al.2021). To ensure proper cooperation between the concrete and steel, connectors would usually be provided between the flanges and at the web(Yan et al. 2025, Liu et al. 2023). The PEC structure has good mechanical properties and fully utilises the advantages of both materials(Liang et al.2019). PEC structures have higher load carrying and deformation capacity for the same section size. In addition, PEC structures can be more easily bolted together and can meet the requirements of rapid construction(Ji et al. 2025,Liang et al.2021).

The application of PEC structures to column members has been relatively well studied. Qian et al.(2023) investigated the compressive behaviour of 8 PEC columns under axial loads and suggested that reducing the spacing of the links could improve the compressive performance. Pereira et al.(2020) performed eccentric compression tests on PEC columns, focusing on the effect of eccentricity. Also, Jamkhaneh et al. (2017) investigated the mechanical behavior of PEC columns under torsional loading and the results showed that the torsional stiffness of PEC columns was maximum at a load ratio of 0.3. Some other scholars have tried PEC columns consisting of new types of concrete (high strength concrete, activated powder concrete, etc.) with main steel components(MSC) and the results showed good load carrying capacity(Xie et al. 2024,Begum et al.2013). Zhu et al. (2025) investigated the mechanical performance of PEC columns after exposure to high temperatures of 900°C. On this basis, Liang et al. (2025) studied the eccentric compression behavior of 6 PEC columns with recycled concrete subjected to different temperatures and eccentricity. In addition, some scholars have conducted finite element analysis of PEC columns (Benedito et al.2023, Wang et al. 2019, Jamkhaneh et al.2020). The above shows that PEC columns are well studied and confirms that PEC columns have good mechanical properties.

However, research on PEC beams has not been neglected. Early in the study, Kindmann et al. (1993) performed static tests on PEC beams and conservatively estimated (without taking into account the contribution of concrete to the compression) the load capacity. Subsequently, Nakamura et al. (2003) compared the bending and shear capacities of PEC beams and steel beams and found that PEC beams were one and two times higher, respectively. Chen et al. (2017) conducted an experimental study on the performance of nine PEC beams under monotonic and cyclic loading and found that the specimens with a shear-to-span ratio of 3.0 had a relatively high load carrying capacity. de Souza et al. (2022) tested the deformation and strength of the PEC beams at the joints with the columns by bolting the beams to the columns. In total, Piloto et al. (2017) performed 27 flexural tests on PEC beams after experiencing different high temperatures, and also analyzed the shear bond conditions between concrete and steel flanges at 400°C. Nardin et al. (2009) mainly investigated the effect of spigot welding location on the overall flexural properties of PEC beams, and found that the layout at the lower flange can increase the flexural load capacity by 10.06% and reduce the relative slip by 35.29%. Chen et al. (2017) found that the loading scenario affects the moment load capacity of PEC beams more than the link spacing and type. The moment redistribution law of PEC beams was investigated by Jiang et al. (2016) and the moment redistribution coefficient was derived. Based on this, some scholars have also launched the finite element analysis and the study of mechanical properties of PEC beams after high temperature(Ahmad et al.2018, Ahn et al. 2017, Jabbar et al.2024).

The above studies, proved the good mechanical properties and good application prospects of PEC structures. PEC beams can somehow replace or due to traditional reinforced concrete beams and steel beams. Existing codes also contain references to PEC beam design(EC4,2004; T/CECS719-2020,2020). However, all existing studies on PEC still retain the configuration of complex longitudinal reinforcement and stirrups, which makes the cross-section of PEC beams complex and difficult to construct(Rana et al. 2018, Ye et al. 2022). Based on this, Liang et al. (2024) and Deng et al.(2025) confirmed that PEC beams still have good mechanical behavior when only the connectors were kept. Wang et al. (2023) solved the section reinforcement congestion problem by opening holes in the MSC. However, PEC beams with openings in the MSC were also investigated by Zhao et al. (2024) but the webs retained the longitudinal reinforcement. The web opening initiative can accommodate the passage of utilities in the building (e.g., firefighting pipes and circuit lines, etc.), but the complex reinforcement retained in the webs in the existing studies prevented the utilization of the web openings to allow the passage of utilities.

Reviewing the above studies, to fulfill the demand of public facilities passing through and also reduce the building height to save cost, this paper proposed a partially wrapped concrete cellular beam (with openings in the MSC) with simplified cross-section reinforcement, as shown in Figure 1. The complex longitudinal reinforcement arrangements have limited the feasibility of openings in the web of beams. In this paper, the flexural performance of PECCB has been evaluated in terms of cellular ratio, cellular geometry, and steel flange thickness of MSC. Finally, this paper also establishes a cracking load prediction model by stress analysis and a deflection prediction model by the discounted web method, respectively. The deflection prediction model was also verified for accuracy by comparing with JGJ 138-2016 and T/CECS719-2020.

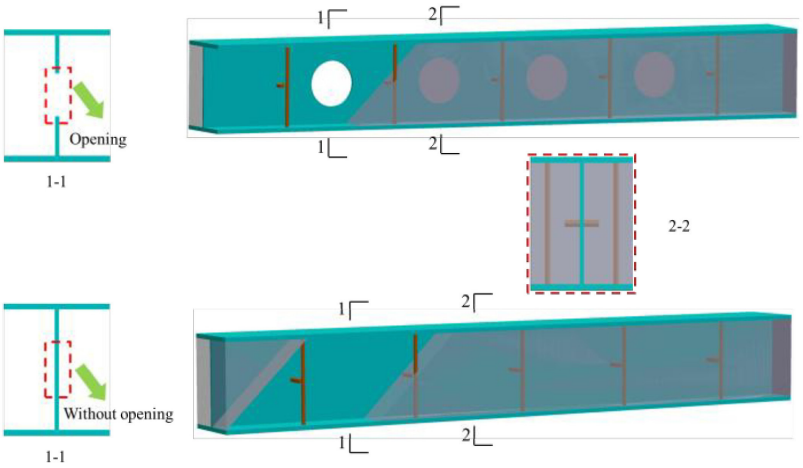

Figure 1 Sketch of PECCB and PECB

2 AIM AND OBJECTIVES

Testing of the flexural behaviour of partially encased concrete cellular beams(PECCBs) is the main research objective of this paper, which focuses on comparing different web opening shapes, cellular rates, flange thicknesses and concrete strengths. In this study, the tests were conducted by applying concentrated loads in the mid-span of PECCBs. A finite element model was also developed to analyse the bending performance of PECCB and compare it with the test results. The main objectives of this paper were as follows:

1. To investigate the cellulars and different cellular shapes on the effectiveness behaviour of PEC beams subjected to flexural behaviour.
2. To observe and analyse the performance of PECCB in flexural behaviour.

3 EXPERIMENTAL INVESTIGATION

3.1 Specimen design and fabrication

For flexural testing, a total of six PECCBs and one PECB were designed in this paper. The details of each beam are displayed in Figure 2 and Table 1. Each specimen beam was 1700mm in length with a clear span of 1400mm and a section size of 150mm x 194mm. All were PECCB except B-9-30, which was a solid PEC beam (control group). The PECCB cellular geometries were circular, square and hexagonal, respectively, with a total of four cellulars in each specimen web. Among them, B-C5-9-30 had 5 cellulars.

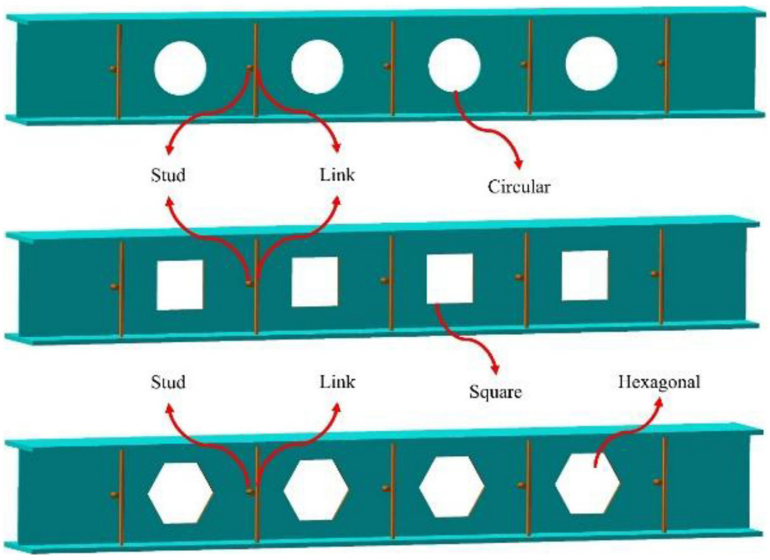

Figure 2 The details of PECCBs.

Table 1 The key parameters of specimen (unit: mm).

Specimen	Cross section		Lower flange thickness	Web cellular		Diameter of connectors		Concrete strength
	b	h	tf2	Shape	Ratio (%)	Stud	Link	
B-C4-4-30	150	194	4	Circular	14.4%	10	8	C30
B-C4-6-30	150	194	6	Circular	14.4%	10	8	C30
B-C4-9-30	150	191	9	Circular	14.4%	10	8	C30
B-S4-9-30	150	189	9	Square	14.4%	10	8	C30
B-H4-9-30	150	194	9	Hexagon	14.4%	10	8	C30
B-C5-9-30	150	194	9	Circular	18.0%	10	8	C30
B-9-30	150	194	9	-	-	10	8	C30

3.2 Material properties

The H-beam used in this test has a nominal strength of 235 MPa and a cross-section geometry of 150 mm × 194 mm, as detailed in Figure 3. Figure 3(a) shows the parameters and cross section of the H-beam used. The steel lower flanges were available in thicknesses of 4, 6 and 9 mm. The flange and web of the H-beam were set up with a set of connectors at 290mm spacing. All the properties of the steel used were tested by GB/T228.1-2021(2021). The results are shown in Table 2. For each batch of concrete, three cubic specimens were prepared for performance testing and measured 32.1 MPa.

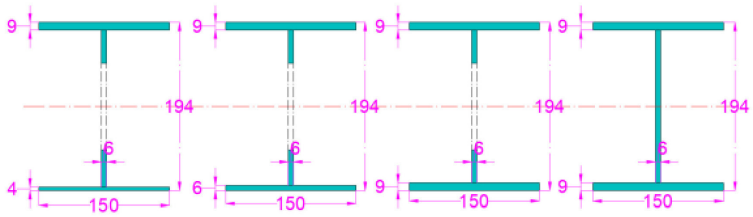

(a) Cross-section of H-beam

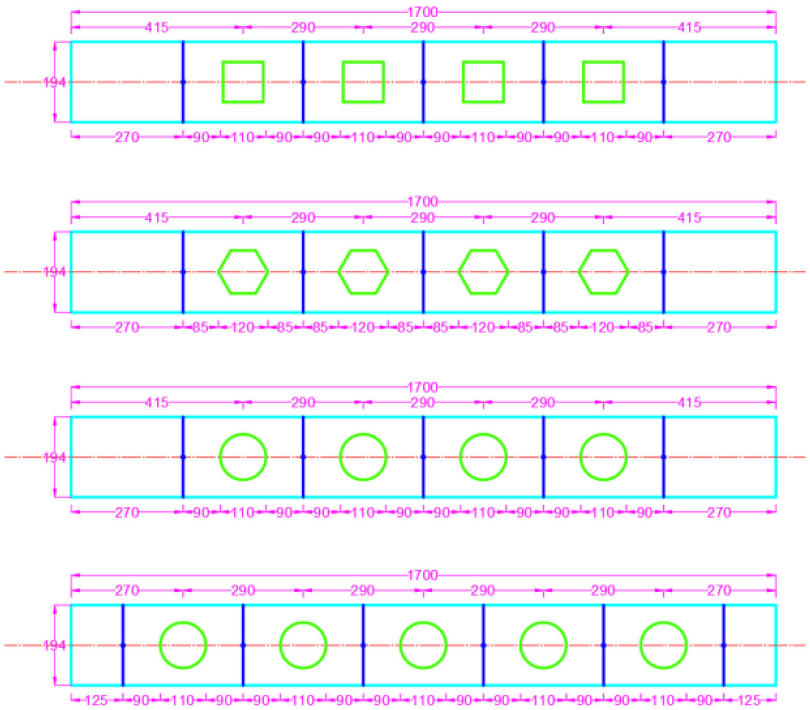

(a) Dimensions of the steel web

Figure 3 The geometry of the specimen.

Table 2 Mechanical properties of steel.

Coupons	Thickness/diameter(mm)	Yield strength fy (MPa)	Tensile strength fu (MPa)	Elasticity modulus Es (GPa)
H-beam	4	321	429	205
	9	320	428	
	6	322	432	
Connectors	8	372	519	201
	10	402	541	202

3.3 Test set-up and instrumentations

The test beams were placed on the loading apparatus of ZT-FY50 using a servo-hydraulic press for four-point bending tests as shown in Figure 4. As shown in Figures 4 and 5, the LVDTs of L1-L3 were distributed in the span of the test beam, and L4 and L5 were distributed at the ends of the beam. The detailed scheme of the measurement point arrangement is also shown in Figure 5. The H-beam web was arranged with strain gauges W1-W6, respectively, and F1-F6 at the lower flange in the span. In addition, the strains at the concrete surface in the span were measured. This loading adopted the mechanism of graded loading, according to GB/T50152-2012(2012) according to each level of 5kN and hold the load for 5min. The cracking load was reached, followed by loading at 20 kN per stage until the specimen was damaged.

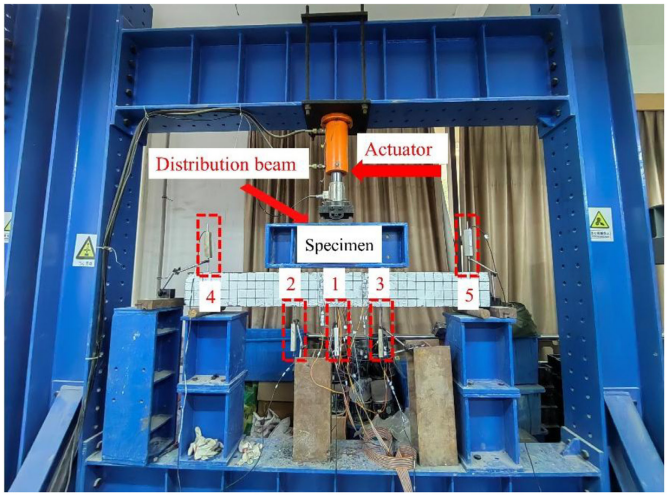

Figure 4 Specimen loading diagram.

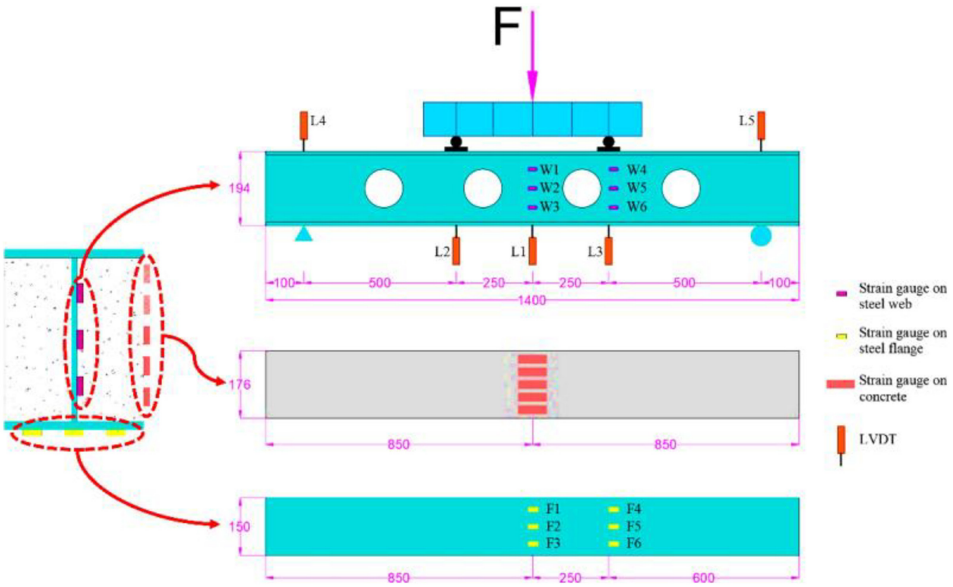

Figure 5 Distribution of measurement points.

4 DISCUSSION AND RESULTS COMPARISON OF TESTED

4.1 Crack and failure patterns

Figure 6 illustrates the final typical failure states of the test beams. Overall, all specimen beams were damaged in the predicted bending condition. At the beginning of loading, there was no significant change in the surface of the specimen. The deflection of the specimen beam was still very small when cracks appeared before reaching the cracking load. As loading continued, some narrow cracks appeared on the concrete surface in the span and deflection increased slowly. The load was further increased to 0.8Mu and the mid-span deflection increased rapidly. With further loading, the concrete cracks increased and compressed concrete was crushed, and the specimen was destroyed. But the specimens with the presence of H-beam showed high ductility. This showed that the web cellular of the H-beam was able to increase the energy dissipation capacity of the specimen beams. The results also confirmed that concrete can inhibit premature buckling of steel flanges, thus increasing the ultimate bearing capacity.

The main manifestations included concrete damage and H-beam buckling. The main forms of damage in PECCB were concrete spalling at the loading points and a concentration of large vertical cracks in the concrete in the span. In addition, the upper flange of the PECCB at mid-span littered with some transverse cracks due to the presence of the web cellular. The control PECB had relatively few vertical cracks and no horizontal cracks, but there were through 45-degree cracks at the support and loading points.

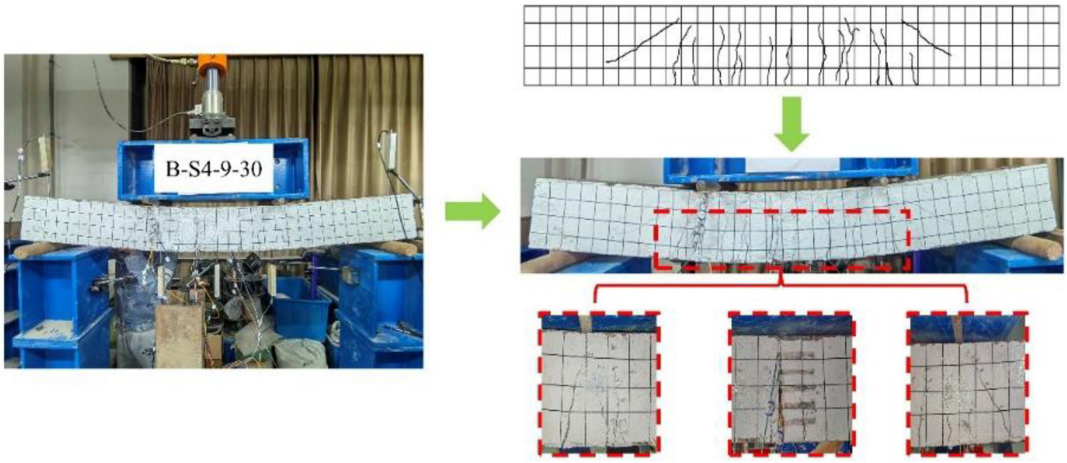

(a) PECCB

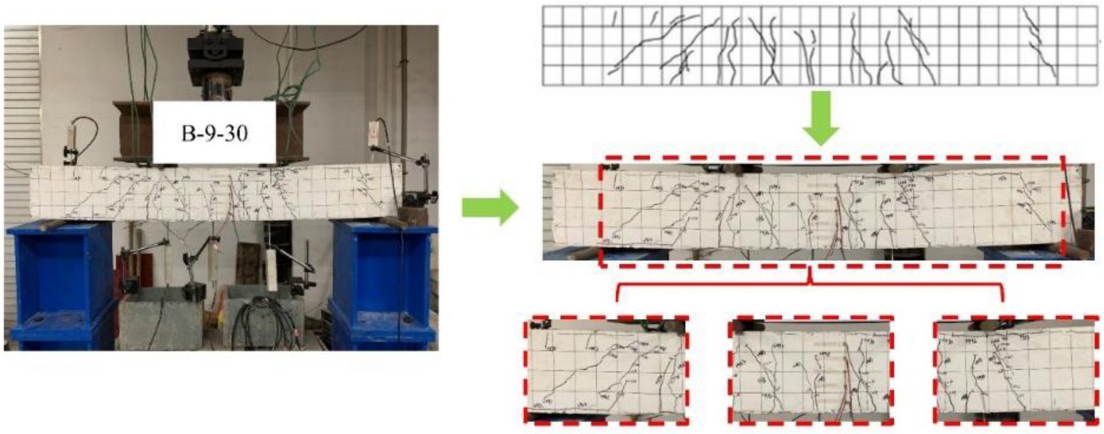

(b) Solid PECB

Figure 6 The typical failure modes.

4.2 Moment Vs deflection behavior

The moment deflection curves of the specimen beams are shown in Figure 7. Bending moments are taken from the numerical multiplication arms of the loading equipment; deflections are taken as the difference between L1 and (L4+L5)/2. All curves were generally similar in morphology and can be divided into a linear phase (P-I), an elastic-plastic phase where the concrete cracks and the H-beam flange begins to buckling (P-II), and a failure phase (P-III). Moments and deflections grow proportionally in the P-I stage, with narrow cracks in the concrete and insignificant mid-span deflections. The growth of the P-II stage curve began to slow down and the concrete indicated widening of the cracks and even a small amount of spalling, with bulging of the steel flanges. The P-III stage curve now rose to the ultimate bending moment and then began to fall, with some spalling of the concrete.

From Figure 7 and Table 3, the slope of the curve was greater for B-9-30 (no cellular). In other words, B-9-30 (no cellular) had more stiffness than PECCB. Comparison of B-9-30 and B-C4-9-30 showed that B-C4-9-30 had better ductility. This showed that the cellular was able to absorb more energy and had a better deformation capacity. However, comparison of B-C4-9-30, B-S4-9-30 and B-H4-9-30 revealed that the circular cellular specimens had the best ductility and good energy dissipation capacity. This indicated that other shapes of cellulars were prone to stress concentrations reducing the performance of the specimen beams(Zhao et al. 2024).

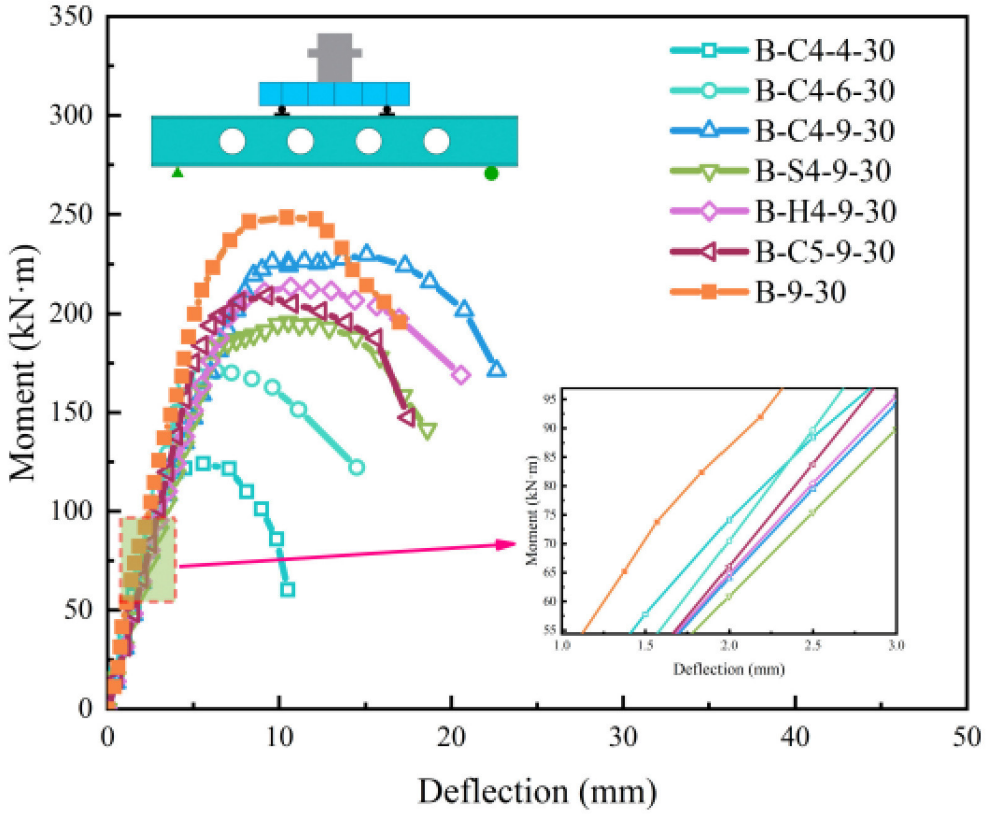

Figure 7 The moment Vs defection behavior.

Table 3 The key results of specimens.

Specimen	Mcr (kN·m)	My (kN·m)	Δy (mm)	Mu (kN·m)	Δu (mm)	Mcr,cal (kN·m)	DI	Mcr,cal/Mcr
B-C4-4-30	18.91	86.93	2.45	124.19	5.56	21.18	2.27	1.12
B-C4-6-30	24.51	119.66	3.25	170.94	8.40	25.25	2.58	1.03
B-C4-9-30	27.14	158.34	5.45	226.20	10.56	26.60	2.61	0.98
B-S4-9-30	25.81	136.99	4.65	195.71	10.52	24.78	2.26	0.96
B-H4-9-30	24.66	147.74	4.87	211.05	10.17	25.65	2.09	1.04
B-C5-9-30	25.17	146.42	4.22	209.17	10.19	25.93	2.41	1.03
B-9-30	35.76	202.78	4.41	248.69	11.01	-	2.50	-

4.3 Strain analysis

Figs. 9 and 10 show the strains in the steel web and concrete of the specimen beams, respectively. Five load level (0.2M_u, 0.4M_u, 0.6M_u, 0.8M_u, 1.0M_u) strain cases are shown in each figure. From Figure 8, the strain in the steel web of the specimen beam exhibits a linear distribution along the height of the section when the bending moment does not exceed 0.6M_u. This coincides with Sections 4.1 and 4.2, indicating that the steel and concrete work in concert during the early stages of loading. When the load reaches 0.8M_u, the value of the measurement point near the flange (W3) increases rapidly, indicating a plastic development stage. In addition, the value of the measuring point near the upper flange (W1) appears to be smaller than the value of the measuring point near the lower flange (W3). This reason can be attributed to the fact that when PEC beams subject to bending, the upper compressive properties as provided by concrete and steel, and the lower tensile properties are provided by steel only. Comparing Figs. 9(a)-9(c), an increasing strain at the web cellular can be observed as the geometry of the cellular changes from circular to hexagonal to square. This also indicates that the stress concentration is most uniform around the perimeter of the circular holes and most severe in the square holes.

The strains on the concrete surfaces of B-C4-9-30 and B-9-30 are illustrated in Figure 9. The strain value of B-C4-9-30 is larger for the same load ratio case. This results from the increased deformation of the concrete caused by the concentration of stress in the cellulars. Figure 10 illustrates the relationship between beam end rotation and strain. PECCB has less flexural stiffness than B-9-30. For B-C4-9-30, B-H4-9-30 and B-S4-9-30, there is little difference in the rotation at the same strain at the beginning of loading. But as the H-beam enters the yielding state, the rotation increases rapidly. Of these, B-H4-9-30 has the fastest rotation increase.

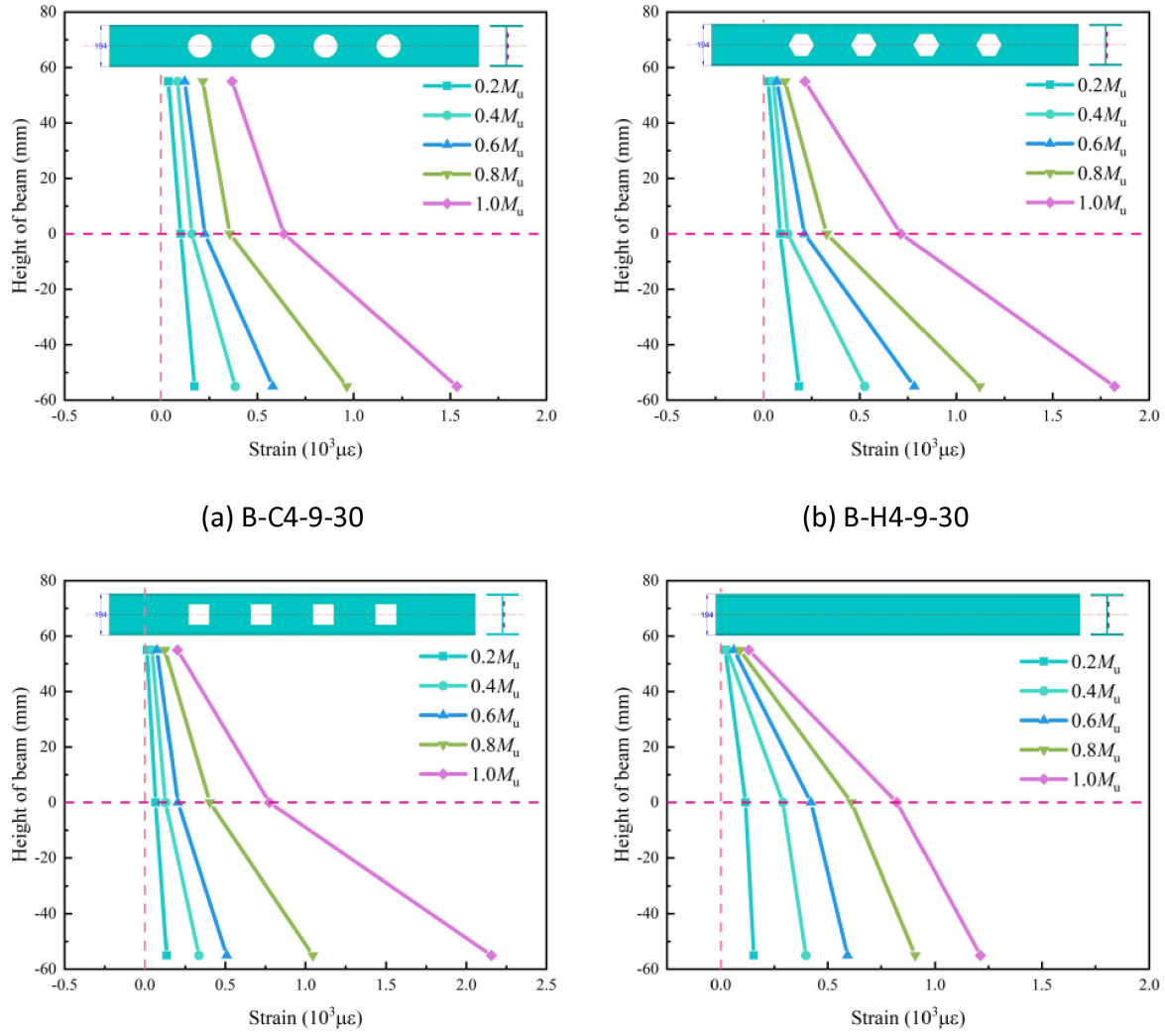

(a) B-C4-9-30 (b) B-H4-9-30

(c) B-S4-9-30 (d) B-9-30

Figure 8 The variation strain of steel web.

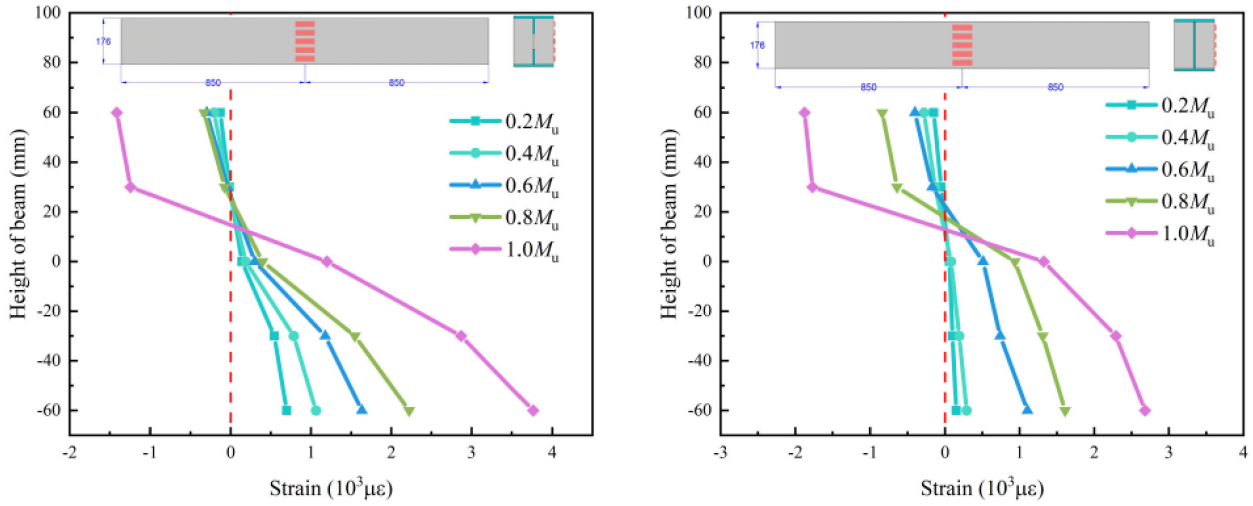

(a) B-C4-9-30 (b) B-9-30

Figure 9 The variation strain of concrete.

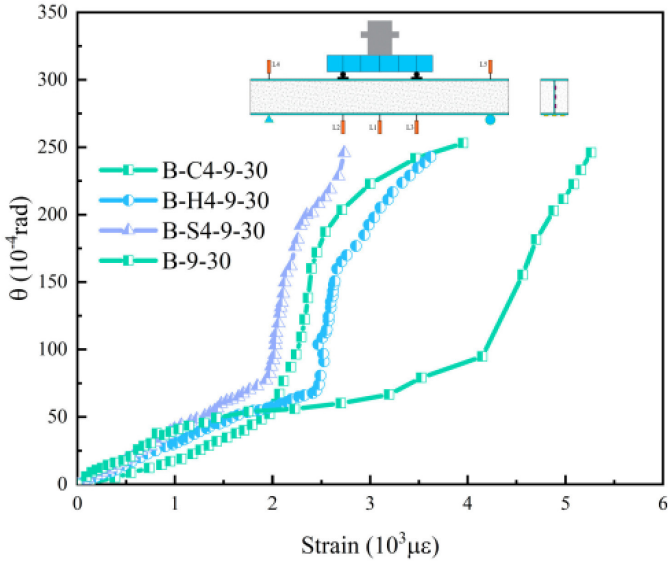

Figure 10 The rotation(θ)-strain(ε) relationship.

5 ANALYTICAL STUDY

5.1 Cracking moment

PECCB during flexure, the upper part of the beam under compression the lower part under tension. The main contribution to the tensile capacity came from steel, with the other part provided by concrete. The stress state of the cross-section of the beam in flexure is shown in Figure 11. The following calculations can be made on the basis of force equilibrium.

$$F_{f,1} + F_{c,1} + F_{w,1} - F_{f,2} - F_{c,2} - F_{w,2} = 0 \tag{1}$$

$$\sigma_{f,c} b_f t_{fu} + 0.5\sigma_{c,c}(b_f - t_w)x_{cr} + 0.5\sigma_{w,c} t_w \frac{x_{cr}}{h_w} x_{cr} = \sigma_{f,t} b_f t_{fl} + \sigma_{c,t}(b_f - t_w)(h_w - x_{cr}) + 0.5\sigma_{w,t} t_w (1 - \frac{x_{cr}}{h_w})(h_w - x_{cr}) \tag{2}$$

Where $F_{f,1}$, $F_{c,1}$ and $F_{w,1}$-Forces on flange, concrete and web in compression zone, respectively; $F_{f,2}$, $F_{c,2}$ and $F_{w,2}$-Forces on flange, concrete and web in tension zone, respectively; $\sigma_{f,c}$, $\sigma_{c,c}$ and $\sigma_{w,c}$-Compressive stress of concrete, flange and steel, respectively; $\sigma_{f,t}$, $\sigma_{c,t}$ and $\sigma_{w,t}$-Tensile stress of concrete, flange and steel, respectively; b_f-Width of flange; x_{cr}-Neutral axis position of cracking load; h_w-Height of web.

Subsequently, the cracking moment (M_{cr}) can be obtained from the definition of bending moment calculation. Where t_w, t_{fu} and t_{f1}-Thickness of web, upper and lower flange, respectively.

$$x_{cr} = \frac{\sigma_{f,t} b_f t_{fl} + f_t(b_f - t_w)h_w + 0.5\sigma_{w,t} t_w h_w - \sigma_{f,c} b_f t_{fu}}{f_t + 0.5\sigma_{c,t}(b_f - t_w) + 0.5(\sigma_{w,t} + \sigma_{w,c})t_w} \tag{3}$$

$$M_{cr} = F_{f,1}(x_{cr} + 0.5t_{fu}) + 0.5F_{c,1}x_{cr} + 0.5F_{w,1}x_{cr} + 0.5F_{c,2}(h_w - x_{cr}) + 0.5F_{w,2}(h_w - x_{cr}) + F_{f,2}(h_w - x_{cr} + 0.5t_{fl}) \tag{4}$$

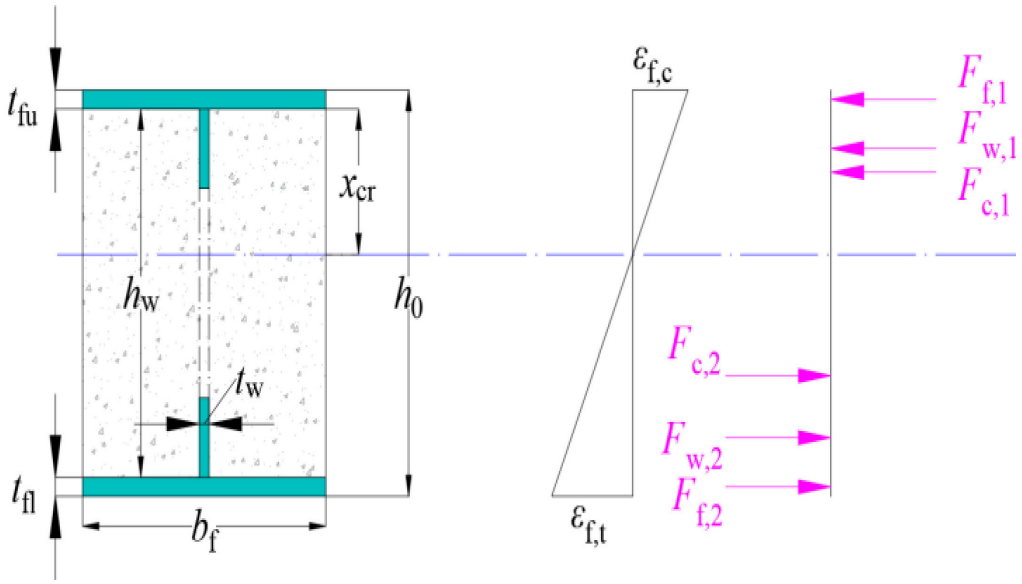

Figure 11 Cross-sectional stress at cracking load.

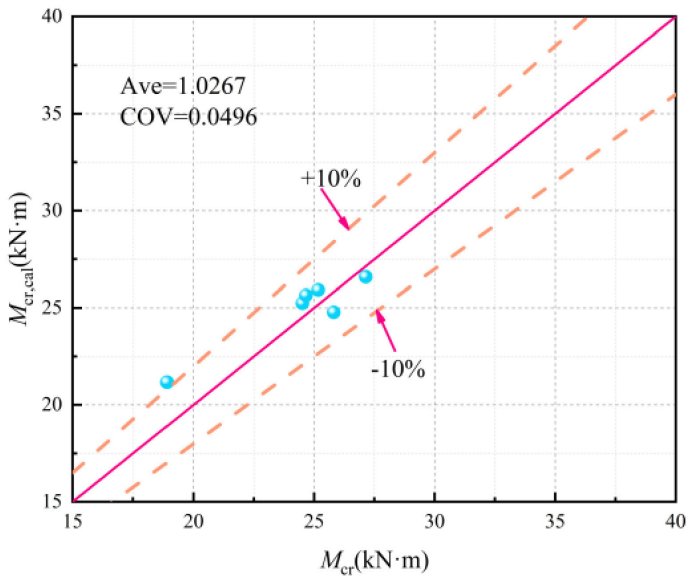

Figure 12 $M_{cr,cal}$ vs M_{cr}.

Table 3 and Figure 12 compare the relationship between the calculated and tested values of cracking loads. The average error of $M_{cr,cal}$ over M_{cr} was 1.0267 and COV was 0.0496. However, the M_{cal} of specimen B-C4-4-30 was 12% larger than the M_{cr}. This may be due to the smaller lower flange, the earlier involvement of the concrete lower flange in tension, and some defects in the quality of the specimen fabrication. These need to be studied further in the future.

5.2 Deflection assessment

The existing codes only give deflection formulas for cellular and PEC beams, and the applicability of PECCB has yet to be assessed. This section evaluates the existing models for the calculation of deflection and makes improvements.

5.2.1 Practical assessment method(Bedford and Liechti,2020)

By evaluating the deflection of a solid web beam of the same dimensions as the cellular beam and multiplying it by an amplification factor(η) as in Eq. (5). Where fsm-Deflection of equal sized normal beam.

$$f = \eta f_{\mathrm{sm}} \tag{5}$$

5.2.2 Fee's Vierendeel truss theory(Russell, 1966)

This method makes up for the defects of the traditional bending moment theory, such as only considering the bending moment deflection, and considers the shear deflection and the deflection under the action of shear sub-bending moment. However, the calculation method is complicated, and the error is large in the case of high span ratio greater than 1/10, not applicable to the actual calculation of the project.

$$f = f_{\mathrm{m}} + f_{\mathrm{v}} + f_{\mathrm{vm}} \tag{6}$$

where f_m, fv, fvm-Flexural deflection, Shear deflection and Shear sub-moment deflection, respectively.

5.2.3 JGJ 138-2016 (2016)

JGJ138-2016 adopts the equivalent stiffness method to superimpose the stiffness (B_s) of the reinforced concrete part and the stiffness of the steel section to calculate.

$$B_s = \left(0.22 + 3.75 \frac{E_a}{E_c} \rho \right) E_c I_c + E_s I_s \tag{7}$$

where E_a, E_c, E_s-Modulus of elasticity of reinforcing steel, concrete and steel section; I_c, I_s-Moment of inertia of concrete and steel section; ρ-Reinforcement ratio of tensile reinforcement.

5.2.4 T/CECS719-2020 (2020)

The equivalent moment of inertia (I_{eq}) of the cross-section is calculated by equating the concrete to a steel cross-section, which is then subjected to the influence of the tensile concrete.

$$I_{\mathrm{eq}} = \frac{I_{\mathrm{ucr}} + I_{\mathrm{cr}}}{2} \tag{8}$$

The discounted stiffness(B) of the beam is then calculated by considering the slip effect.

$$B = \frac{E_{\mathrm{s}} I_{\mathrm{eq}}}{1 + \zeta} \tag{9}$$

$$\zeta = \eta\left[0.4 - \frac{3}{(jl)^2}\right] \tag{10}$$

$$\eta = \frac{36E_s d_c p A_0}{n_s k h l^2} \tag{11}$$

$$j = 0.81\sqrt{\frac{n_s N_v^c A_1}{E_a I_0 \rho}} \tag{12}$$

Therefore, the equivalent moment of inertia(I_0) and equivalent cross-sectional area(A0) are as in Eqs. (13-14). The I0 and A0 ratio(A1) is shown in Eq. (15).

$$I_0 = I_s + \frac{I_{cf}}{\alpha_E} \tag{13}$$

$$A_0 = \frac{A_{cf} A_s}{\alpha_E A_s + A_c} \tag{14}$$

$$A_1 = \frac{I_0 + A_0 d_c^2}{A_0} \tag{15}$$

Where ζ-Discount factor for *B*; I_{ucr}, I_{cr}-Converted section moments of inertia for uncracked and cracked sections of the beam; *h*-Height of beam; *l*-Length of beam; n_s, *p*, *k*-Number of columns, spacing and stiffness factor of connectors; N_v^c-Bearing capacity of the connectors; α_E-Ratio of modulus of elasticity of steel to concrete; I_s, I_{cf}-Moment of inertia of steel and concrete section; d_c-Distance between the centre of form of steel section and the centre of form of concrete.

From Fig. 13, the deflection of the beam is calculated in the following equation for the methods introduced in Sections 5.2.3 and 5.2.4.

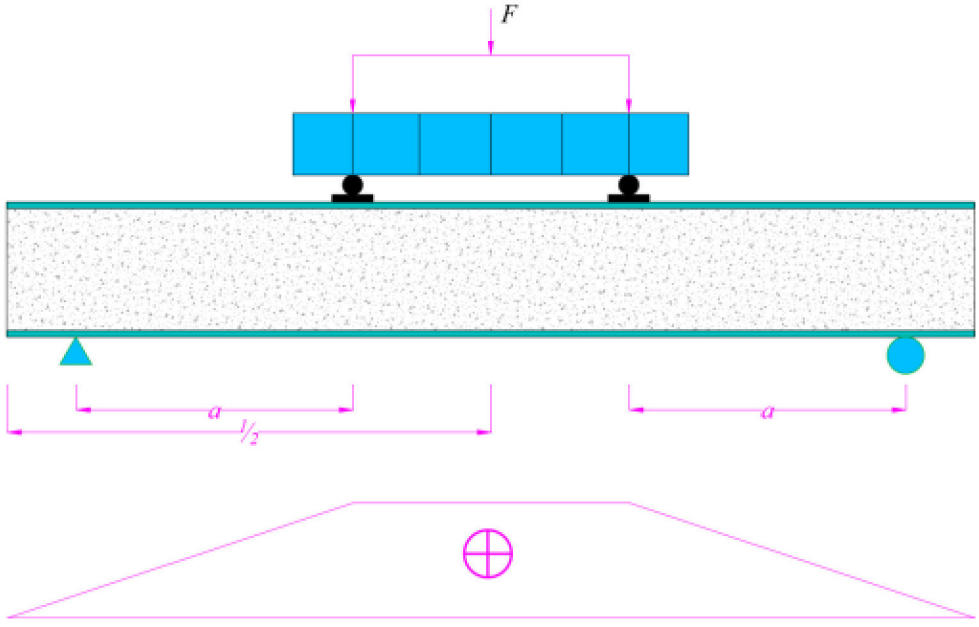

Figure 13 Sketch of PECCB flexural calculation.

$$f = \sum \int \frac{\overline{MM_P}}{B} dx = \frac{Fa}{24B}(3l^2 - 4a^2) = \frac{23Fl^3}{648B} \tag{16}$$

The calculation results of JGJ138-2016 and T/CECS719-2020 are shown in Figure 14 and Table 4. Both calculated values were less than the tested values and the mean values were 0.81 and 0.64, respectively. All these codes overestimate the flexural stiffness of the beams, making the calculation results small. Therefore, improvements are needed. The moments of inertia of the adjusted beam as,

$$\begin{aligned} I_s &= I_{f1} + I_w + I_{f2} \\ &= \frac{b_f t_{fu}^3}{12} + a_{f1}^2 b_f t_{fu} + \frac{h_w t_{wc}^3}{12} + a_w^2 h_w t_{wc} + \frac{b_f t_{fl}^3}{12} + a_{f2}^2 b_f t_{fl} \end{aligned} \tag{17}$$

Among, t_{wc} is based on the discounted web thickness of Liang (2024) and Wang (2023) as follows.

$$t_{wc} = \left(\frac{S_w - S_c}{S_w}\right) t_w \tag{18}$$

Where a_{fl}-Distance between upper and lower flange centres and neutral axis; a_w-Distance between web centre and neutral axis. S_w, S_c-Area of steel web and cellular.

Table 4 Deflection calculation results. unit: mm.

ID	f1	f2	f3	ft	f1/ ft	f2/ ft	f3/ ft
PECCB-C4-4-30	2.50	1.68	2.07	2.21	1.13	0.58	0.94
PECCB-C4-6-30	2.65	1.95	3.02	2.94	0.90	0.51	1.03
PECCB-C4-9-30	3.22	2.75	4.25	4.67	0.69	0.59	0.91
PECCB-S4-9-30	2.83	2.41	3.73	4.10	0.69	0.59	0.94
PECCB-H4-9-30	3.04	2.59	4.01	4.26	0.71	0.61	0.91
PECCB-C5-9-30	2.94	2.51	3.95	3.87	0.76	1.14	1.02
Mean					0.8133	0.6700	0.9583
SD					0.1590	0.2125	0.0488

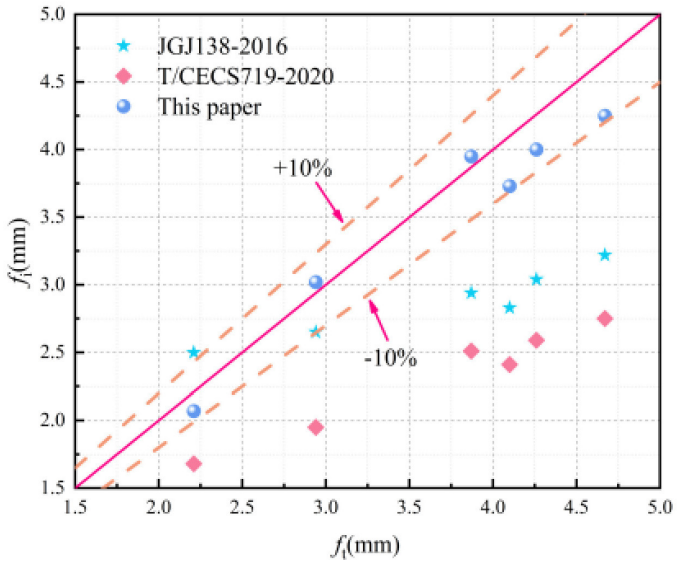

Figure 14 f_i vs. f_t. (i=1, 2, 3)

From Figure 14, the calculated values of the deflection prediction model proposed in this paper have an average of 0.958 over the deflection test values. The maximum error was only 9.0% with a standard deviation(SD) of 0.045, giving good predictive accuracy.

6 CONCLUSION

This paper has investigated the mechanical behaviour of a novel PECCB subjected to four-point flexure. This paper focused on analysing the PECCB as affected by the cellular geometry (circular, square, hexagonal), the cellular ratio(14.4%, 18.0%) and the lower flange thickness(4, 6, 9mm) parameters. Following testing and analysis, analytical models were developed. The main calculations were for cracking loads, deflection and flexural strength. Based on the above, it can be concluded:

1. The PECCB studied in this paper possesses a higher energy dissipation capacity than the conventional PECB. The damage of PECCB can generally be characterised by flange buckling and concrete crushing.
2. The slopes of the bending moment deflection curves of PEECB are all smaller than those of PECB. In other words, the web cellular reduces the ability of the PEECB to resist deformation and the stiffness is reduced by about 6.18% on average. The stiffness of the square cellular specimen decreased the most for the same cellular ratio.
3. Before $0.6M_u$, the strain in the steel web of PECCB varied linearly at different heights. There were stress concentrations around the web honeycomb, causing the concrete to indicate increased strain, with the square stress concentrations being the most obvious. Therefore, square cellular won't be recommended for practical applications.
4. The cracking load calculation model based on the stress state of the cross-section predicted the cracking load of the PECCB well with an error mean and COV of 1.0267 and 0.0496, respectively.
5. An analytical model of PECCB deflection was developed by discounting the web thickness, and the average error between the calculated and tested values was 0.958 with an SD of 0.045.

Acknowledgements

The authors are grateful to the financial support provided by the National Natural Science Foundation of China (No. 52068001), the Key Project of Jiangxi Provincial Natural Science Foundation (No. 20252BAC250054).

Author's Contribuitions: Qiuyu Liu: Writing – review & editing, Resources, Formal analysis, Conceptualization. **Jiongfeng Liang:** Writing – review & editing, Supervision, Resources, Project administration, Funding acquisition. **Bin Zou:** Writing – review & editing, Resources, Supervision**,** Methodology. **Caisen Wang:** Writing – review & editing, Writing – original draft, Investigation, Data curation. **Shengzhi Shi:** Writing – review & editing, Visualization, Resources, Formal analysis. **Kai Wang:** Resources, Methodology, Investigation, Data curation

Data Availability: Research data is only available upon request

Editor: Marco L. Bittencourt

References

Ebadi Jamkhaneh, M., Kafi, M. A., & Kheyroddin, A. (2019). Behavior of partially encased composite members under various load conditions: Experimental and analytical models. Advances in Structural Engineering, 22(1), 94-111.

Mucedero, G., Brunesi, E., & Parisi, F. (2021). Progressive collapse resistance of framed buildings with partially encased composite beams. Journal of Building Engineering, 38, 102228.

Yan, W., Yang, Y., Lou, G., & Chen, Y. F. (2025). Behavior of shear connection in web-embedded U-shaped steel-concrete composite beams: Experimental and numerical study. Engineering Structures, 332, 120020.

Liu, X., Bi, Z., Hu, J., Hao, H., Lin, Z., Li, H., ... & Yang, G. (2023, December). Bolted shear connectors in steel–concrete composite structures: Shear behavior. In Structures (Vol. 58, p. 105524). Elsevier.

Liang, J., Zhang, G., Wang, J., & Hu, M. (2019). Mechanical behaviour of partially encased composite columns confined by CFRP under axial compression. Steel and Composite Structures, An International Journal, 31(2), 125-131.

Ji, Y. P., Hu, H. S., Peng, B., & Skalomenos, K. (2025). Compressive behavior of partially prefabricated concrete-encased-and-filled steel tubular columns. Engineering Structures, 333, 120129.

Liang, J. F., Zhang, L. F., Yang, Y. H., & Wei, L. (2021). Flexural behavior of partially prefabricated partially encased composite beams. Steel and Composite Structures, An International Journal, 38(6), 705-716.

Qian, Z., Wang, J., Liu, Y., & Xu, Q. (2023). Axial compressive performance of partially encased steel-concrete composite stub columns filled with lightweight aggregate concrete. Engineering Structures, 291, 116422.

Pereira, M. F., De Nardin, S., & El Debs, A. L. H. C. (2020). Partially encased composite columns using fiber reinforced concrete: experimental study. Steel and Composite Structures, 34(6), 909-927.

Jamkhaneh, M. E., & Kafi, M. A. (2017). Experimental and numerical investigation of octagonal partially encased composite columns subject to axial and torsion moment loading. Civil Engineering Journal, 3(10), 939-955.

Xie, Y. T., Wang, J. X., Wang, Y. Z., Zhang, B. J., & Wang, S. Y. (2024). Axial compressive behavior of partially encased composite reactive powder concrete columns after high-temperature exposure. Case Studies in Construction Materials, 21, e03625.

Begum, M., Driver, R. G., & Elwi, A. E. (2013). Behaviour of partially encased composite columns with high strength concrete. Engineering Structures, 56, 1718-1727.

Zhu, Y., Du, H., Liu, C., Yang, H., Wang, Y., & Xu, L. (2025). Performance of partially encased composite stub columns after high-temperature exposure. Journal of Constructional Steel Research, 227, 109308.

Liang, J., Luo, X., Wang, C., & Li, W. (2025, March). Study on eccentric compression performance of partially encased recycled concrete columns after high temperature. In Structures (Vol. 73, p. 108378). Elsevier.

Benedito, A. V., Milani, M. F. P., Krahl, P. A., Marques, B. B., De Nardin, S., & Martins, C. H. (2023, December). Nonlinear finite element analysis of partially encased composite columns under non-uniform moments. In Structures (Vol. 58, p. 105519). Elsevier.

Wang, H., Li, J., & Song, Y. (2019). Numerical study and design recommendations of eccentrically loaded partially encased composite columns. International Journal of Steel Structures, 19(3), 991-1009.

Jamkhaneh, M. E., Ahmadi, M., & Sadeghian, P. (2020). Simplified relations for confinement factors of partially and highly confined areas of concrete in partially encased composite columns. Engineering Structures, 208, 110303.

Kindmann, R., Bergmann, R., Cajot, L. G., & Schleich, J. B. (1993). Effect of reinforced concrete between the flanges of the steel profile of partially encased composite beams. Journal of Constructional Steel Research, 27(1-3), 107-122.

Nakamura, S. I., & Narita, N. (2003). Bending and shear strengths of partially encased composite I-girders. Journal of constructional steel research, 59(12), 1435-1453.

Chen Yiyi, Li Wei, & Fang Cheng. (2017). Performance of Partially Encased Composite Beams Under Static and Cyclic Bending. Structures, 9, 29-40.

de Souza Spavier Patricia T., & El Debs Ana Lucia H. C. (2022). Experimental analysis of beam-to-column connection with partially encased concrete column with varying inertia axis. Journal of Constructional Steel Research, 194, 107325.

Piloto, P. A., Ramos-Gavilán, A. B., Gonçalves, C., & Mesquita, L. M. (2017). Experimental bending tests of partially encased beams at elevated temperatures. Fire Safety Journal, 92, 23-41.

De Nardin, S., & El Debs, A. L. H. (2009). Study of partially encased composite beams with innovative position of stud bolts. Journal of Constructional Steel Research, 65(2), 342-350.

Jiang, Y., Hu, X., Hong, W., & Wang, B. (2016). Experimental study and theoretical analysis of partially encased continuous composite beams. Journal of Constructional Steel Research, 117, 152-160.

Ahmad, S., Masri, A., & Abou Saleh, Z. (2018). Analytical and experimental investigation on the flexural behavior of partially encased composite beams. Alexandria engineering journal, 57(3), 1693-1712.

Ahn, J. K., & Lee, C. H. (2017). Fire behavior and resistance of partially encased and slim-floor composite beams. Journal of Constructional Steel Research, 129, 276-285.

Jabbar, A. M., Al-Zuheriy, A. S. J., & Hasan, Q. A. (2024, December). A numerical investigation of the structural behavior of reinforced concrete beams fully or partially encased with UHPC layers in flexure. In Structures (Vol. 70, p. 107706). Elsevier.

Eurocode 4, EN 1994-1-1: design of composite steel and concrete structures- part1-1 general rules and rules for buildings. European Committee for Standardization; 2004.

Technical specification for partially-encased composite structures of steel and concrete (T/CECS719-2020). Beijing: China Association for Engineering Construction Standardization; 2020. [in Chinese].

Rana, M. M., Lee, C. K., Al-Deen, S., & Zhang, Y. X. (2018). Flexural behaviour of steel composite beams encased by engineered cementitious composites. Journal of constructional steel research, 143, 279-290.

Ye, Y., Yao, Y., Liao, H., Xin, L., & Liu, Y. (2022). Flexural performance of hollow-core partially-encased composite beams. Journal of Building Engineering, 45, 103432.

Liang, J., Zou, W., Wang, C., & Li, W. (2024, June). Flexural performance of partially encased steel-concrete composite beams with web opening. In Structures (Vol. 64, p. 106666). Elsevier.

Deng, Z., Liang, J., Wang, C., & Wang, L. (2025, August). Research on shear performance of web opening partially encased concrete composite beams. In Structures (Vol. 78, p. 109327). Elsevier.

Wang, N., Hou, H., Wang, Y., Qu, B., Zeng, X., Fang, H., ... & Xiong, F. (2023). Flexural behavior of partially encased cellular beams: Tests and design implications. Engineering Structures, 293, 116631.

Zhao, B., Huo, H., Ran, C., Fang, C., Wang, W., & Zhou, H. (2024). Flexural behavior of castellated partially encased composite (PEC) beams. Journal of Constructional Steel Research, 214, 108509.

Metallic materials-Tensile testing-Part 1: Method of test at room temperature (GB/T 228.1–2021). Beijing: General Administration of Quality Supervision, Inspection and Quarantine of the People's Republic of China; 2021. [in Chinese].

Standard for test method of concrete structures (GB/T 50152-2012). Beijing: General Administration of Quality Supervision, Inspection and Quarantine of the People's Republic of China; 2012. [in Chinese].

Bedford, A., & Liechti, K. M. (2020). Deflections of beams. In Mechanics of Materials (pp. 671-728). Cham: Springer International Publishing.

Russell, W. C. (1966). Experimental studies of Vierendeel beam analysis.

Code for design of composite structures (JGJ/138-2016). Beijing: China Engineering Construction Standardization, Association; 2016. [in Chinese].

Technical Specification for Partially- Encased Composite Structures of Steel and Concrete (T/CECS719-2020). Beijing: China Association for Engineering Construction Standardization; 2020. [in Chinese].